Revolutionizing Igneous Rock Classification: Proportion-Based Deep Learning Analysis of Petrographic Thin Section Photomicrographs

Evelyn Jessica Jaya[1], Xinbing Wang[1], Chenghu Zhou[1], and Nanyang Ye[1]

[1]*Shanghai Jiao Tong University, Shanghai, China (evelyn321jaya@gmail.com)*

EGU General Assembly #EGU24 14-19 April 2024

1. Introduction

- Geological research has long relied on the meticulous examination of thin section photomicrographs for the classification of igneous rocks. However, traditional petrographic methods are often marred by subjectivity and observer variability, hindering the precision and reproducibility of rock classification.
- The cornerstone of our methodology lies in recognizing the intimate relationship between the mineral composition of rocks and their classification. Our method prioritizes the accurate quantification of mineral proportions within thin section photomicrographs.

- The determination of the major categories should be based on chemical composition and mineral composition.
- The naming of the second and third levels should be based on mineral composition and structure, etc.

↓

supplementary names based on minor minerals should be added before the basic name of the rock.

↓

E.g. 云闪花岗岩(Dolomite-quartz granite) contains more 角闪石(Amphibole) than 黑云母(Biotite)

Fig 1. The overall naming process of rocks

2. Data Preparation

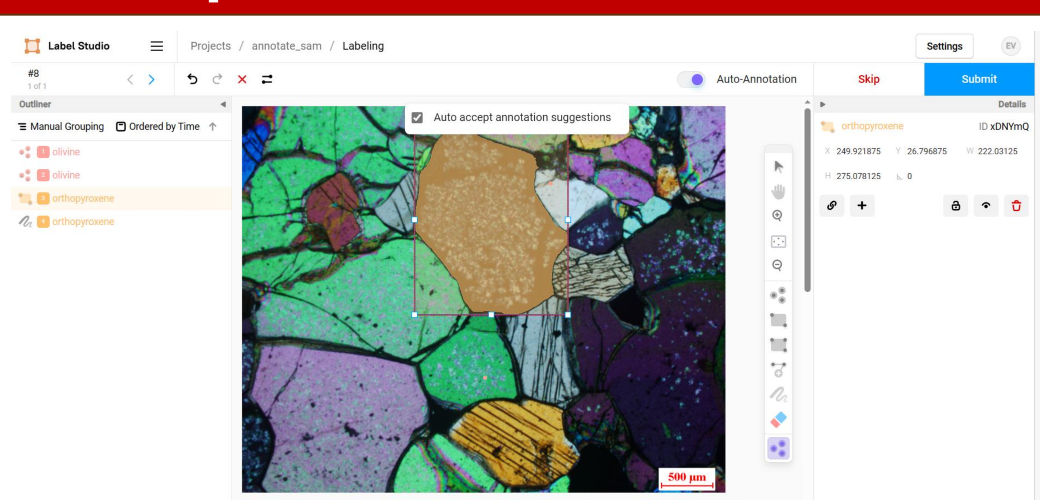

Fig 2. Semi-automated Labelling process with label studio

- Our study leverages semantic image segmentation to analyze 963 petrographic thin section photomicrographs, identifying 29 distinct minerals and classifying 15 types of igneous rocks.
- We conducted manual annotation of the image to generate the corresponding mask. The integration of the pre-trained ViT-Base Segment-Anything Model (SAM) into Label Studio significantly augmented the efficiency of the annotation workflow.
- It is imperative to acknowledge that the predominant challenges encountered during this process involved identifying certain obscure regions, thereby leading to incomplete annotation.

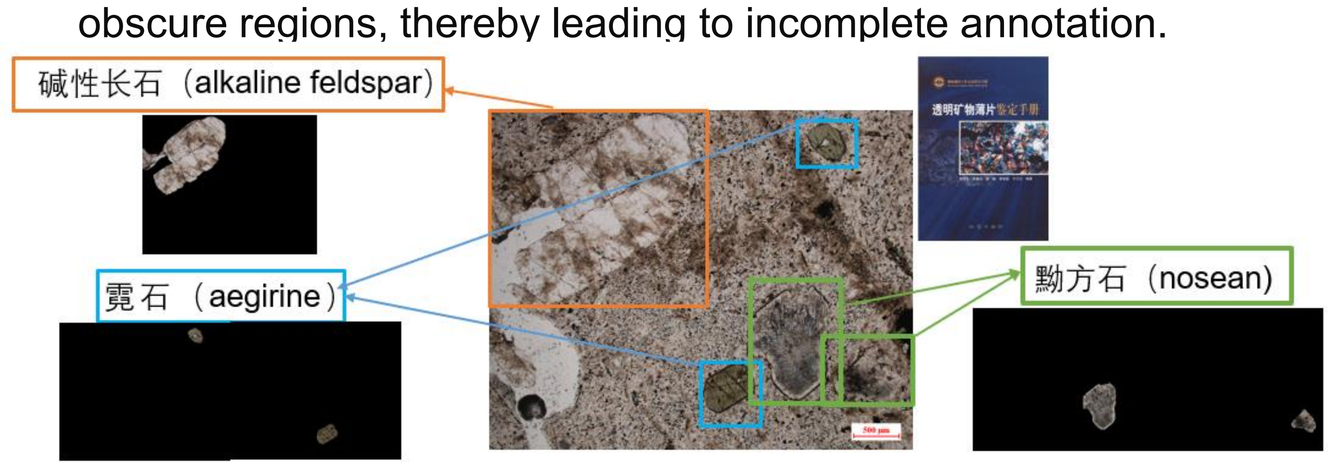

Fig 3. An example of mineral object identification in the labeling process

3. Methodology

Mineral	Number of Samples	Total Pixels
Aegirine	31	208887
Aegirine Augite	25	360232
Alkaline Feldspar	614	73628253
Apatite	85	1668436
Arfvedsonite	71	16446522
Biotite	361	5459905
Calcite	43	1197511
Chloritic Pyroxene	236	2738250
Clinopyroxene	258	4660213
Feldspar	55	6745883
Hornblende	315	18801770
Hypersthene	167	5172164
Ilmenite	39	449445
Mica	49	231821
Muscovite	47	1855608
Nepheline	111	10936058
Nosean	44	2236053
Olivine	420	27499234
Orthoclase	73	11053376
Orthopyroxene	49	1804539
Phlogopite	67	1225798
Plagioclase	1341	46851825
Pyroxene	67	1225798
Quartz	535	37011962
Sanidine	60	4010568
Sodalite	3	11106
Spinel	43	138114
Titanaugite	51	13717797
Zircon	22	526531

Table 1. The distribution of labeled minerals identified within the image, revealing a significant imbalance among the 29 mineral classes.

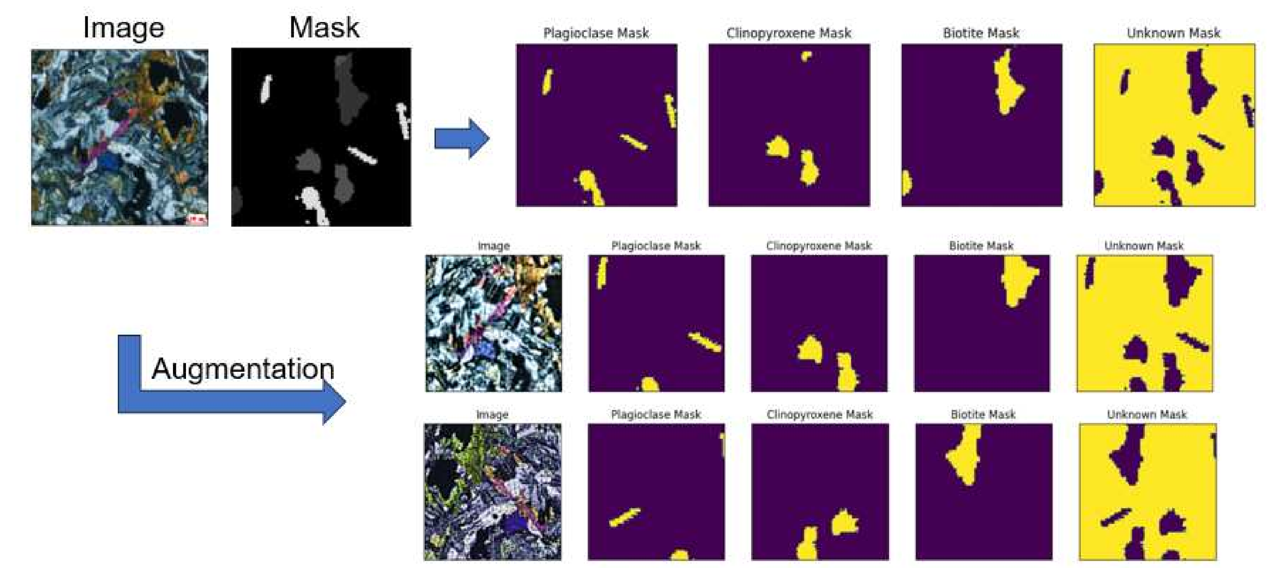

- Robust data augmentation techniques including spatial shifts, image flips, cropping, padding, Gaussian noise, and blurring were implemented.
- Resampling techniques were employed to address the inherent imbalance in the dataset, ensuring a more equitable distribution of mineral classes.
- One-hot encoding strategy was adopted to focus the model's attention solely on the 29 recognized mineral classes, thereby avoiding engagement with unknown complexities

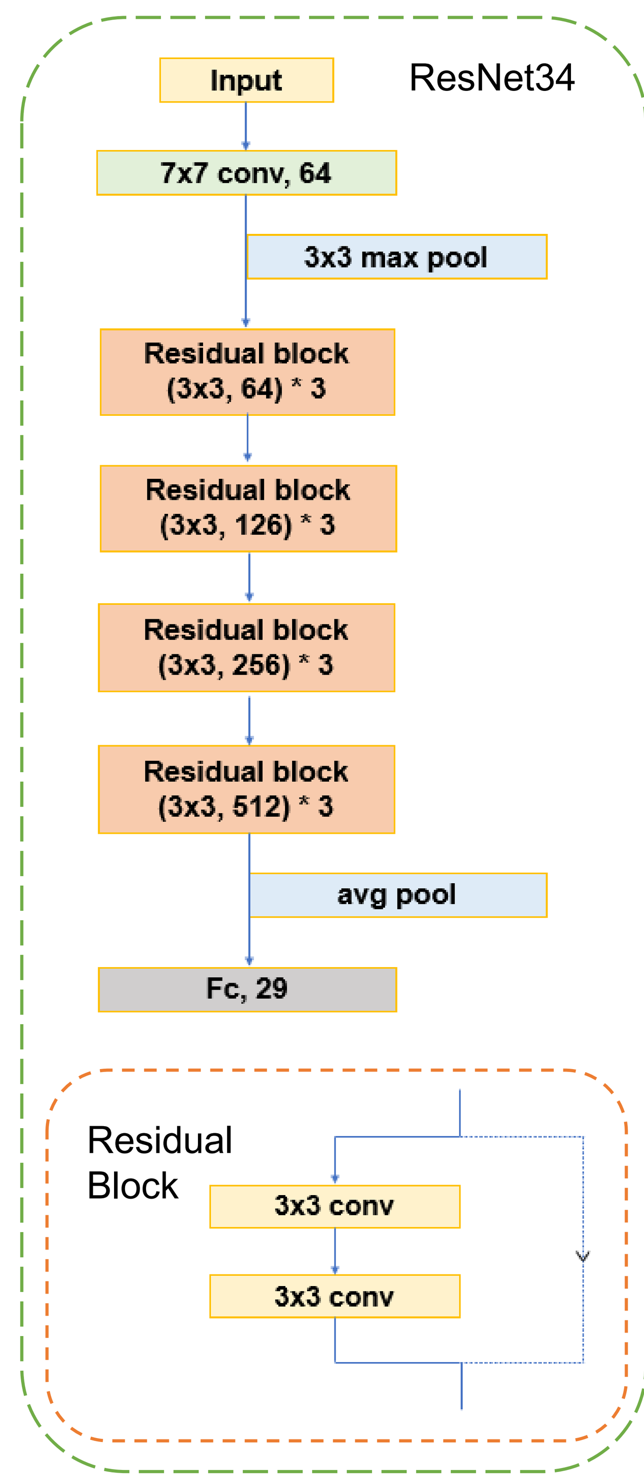

Semantic Segmentation

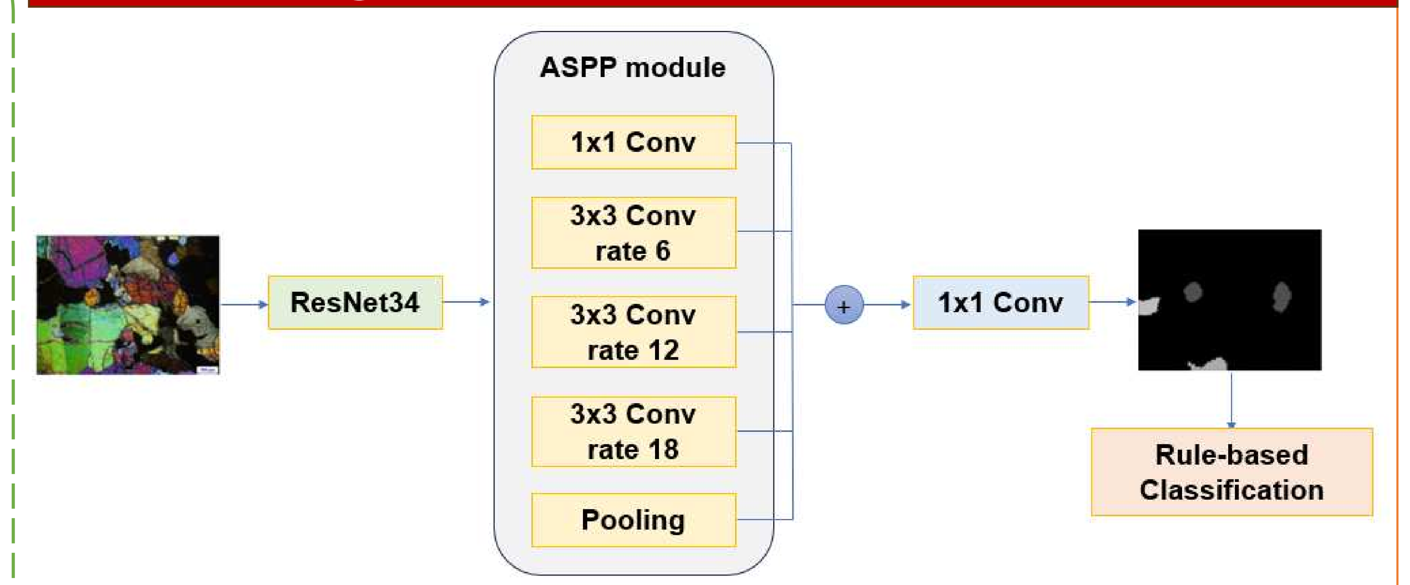

- Transfer learning with Resnet34 as the encoder was employed to improve feature extraction
- The dataset was divided into training, validation, and testing sets in a 70:20:10 ratio, with training spanning 20 epochs using the Adam optimizer with a learning rate of 1e-5.

Power Jaccard Loss

$$J_p(y,\hat{y},p) = 1 - \frac{(y\cdot\hat{y})+\varepsilon}{(y^p+\hat{y}^p-y\cdot\hat{y})+\varepsilon}$$

Power Jaccard Loss incorporates a power term p (must be a value between 0 and 1) into the standard Jaccard loss equation to amplify the impact of incorrect predictions during the training process.

4. Results

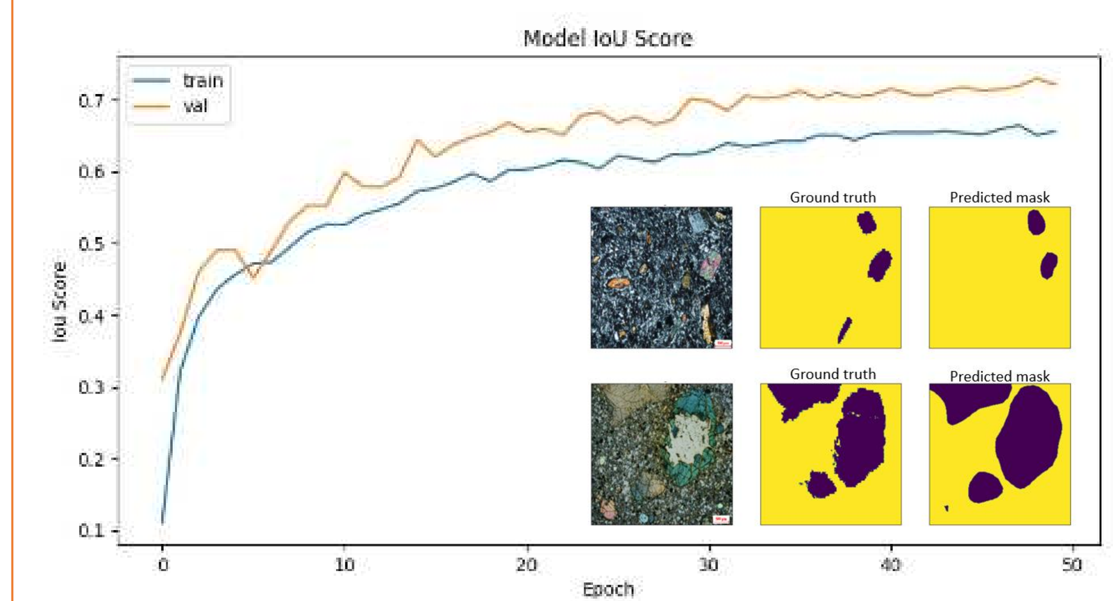

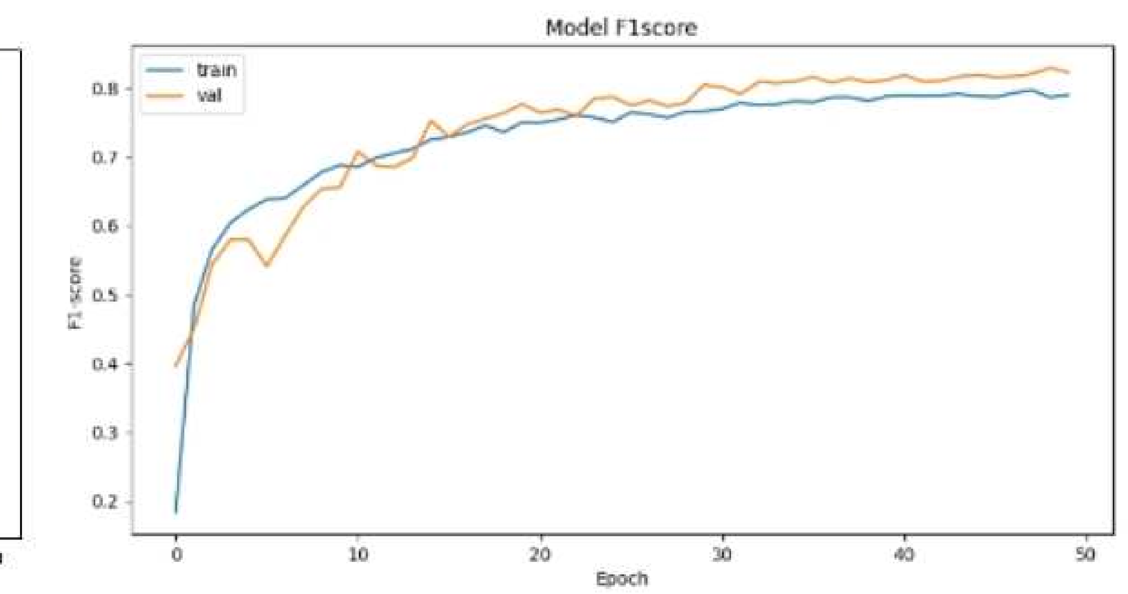

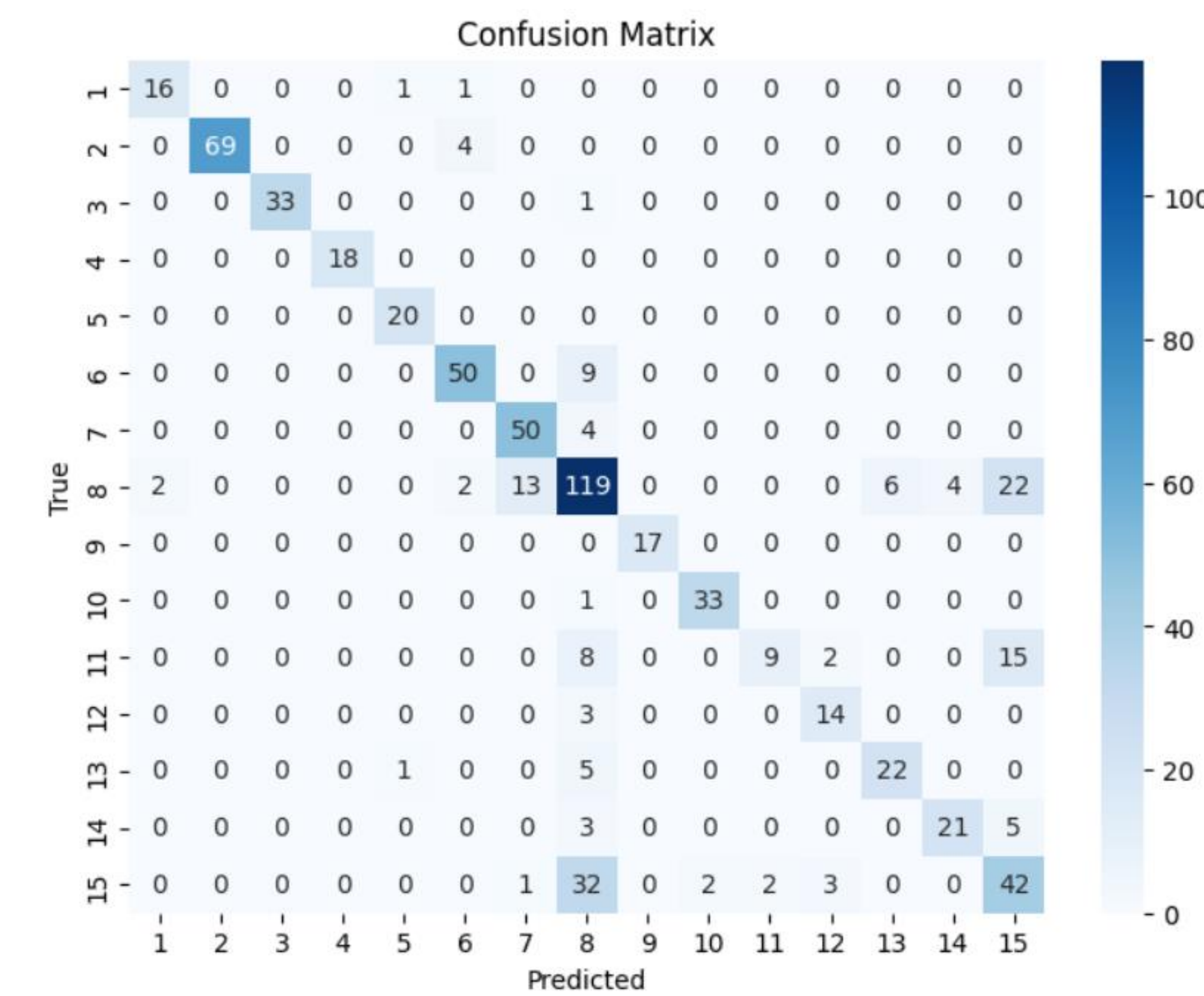

Class	Igneous Rocks
1	Kimberlite
2	Peridotite
3	Syenite
4	Titanite
5	Calcite
6	Pyroxenite
7	Anorthosite
8	Feldspar
9	Trachyte
10	Nephelinite
11	Quartzite
12	Nosean phonolite
13	Amphibolite
14	Minette
15	Granite

- Despite the challenges posed by incomplete labeling in the dataset, Our approach was able to achieve a classification accuracy of **73.32%**. Our method surpasses the baseline method using VGG16 as the backbone, which attains only
- 63.64% classification accuracy. This suggests that even with incomplete labeling, Our method demonstrated robustness and effectiveness in accurately quantifying mineral proportions and classifying igneous rocks.

5. Conclusions

We introduce a novel approach to classifying igneous rocks through segmented-based, rule-driven analysis of thin section photomicrographs. By employing deep learning and semantic image segmentation, the method accurately quantifies mineral proportions, addressing subjectivity and variability in traditional petrography. We had successfully identify 29 minerals and classifies 15 types of igneous rocks across 963 photomicrographs, achieving a classification accuracy of 73.32%. This approach not only improves rock classification precision but also signifies a significant advancement in geological research by integrating advanced image processing with deep learning, paving the way for new frontiers in Earth sciences.

EGU European Geosciences Union · Deep-time Digital Earth · IUGS · 上海交通大學 SHANGHAI JIAO TONG UNIVERSITY